Published in final edited form as:

Cancer Discov. 2019 July ; 9(7): 944–961. doi:10.1158/2159-8290.CD-18-1393.

Mechanisms of lymphoma clearance induced by high-dose alkylating agents

Chen Lossos[1], **Yunpeng Liu**[2,3], **Kellie E. Kolb**[2,4,5], **Amanda L. Christie**[1], **Alexandria Van Scoyk**[1], **Sanjay M. Prakadan**[2,4,5], **Kay Shigemori**[1], **Kristen E. Stevenson**[1], **Sara Morrow**[1], **Olivia D. Plana**[1], **Cameron Fraser**[6,7], **Kristen L. Jones**[1], **Huiyun Liu**[1], **Christian P. Pallasch**[8], **Rebecca Modiste**[9], **Quang-De Nguyen**[9], **Jeffrey W. Craig**[10], **Elizabeth A. Morgan**[10], **Francisco Vega**[11], **Jon C. Aster**[10], **Kristopher A. Sarosiek**[6,7], **Alex K. Shalek**[2,4,5], **Michael T. Hemann**[2,3], and **David M. Weinstock**[1,2]

[1]Department of Medical Oncology, Dana-Farber Cancer Institute and Harvard Medical School, Boston, MA, 02215, USA.

[2]Broad Institute of MIT and Harvard University, Cambridge, Massachusetts, 02142, USA.

[3]MIT Koch Institute for Integrative Cancer Research, 500 Main St, Cambridge MA 02142.

[4]Institute for Medical Engineering and Science (IMES), Department of Chemistry, and Koch Institute for Integrative Cancer Research, MIT, Cambridge, MA, USA.

[5]Ragon Institute of MGH, MIT and Harvard, Cambridge, MA, USA.

[6]John B. Little Center for Radiation Sciences, Department of Environmental Health, Harvard T.H. Chan School of Public Health, Boston, MA 02115.

Corresponding author: David Weinstock, Dana-Farber Cancer Institute, 450 Brookline Avenue, Dana 510B, Boston, MA 02215. davidm_weinstock@dfci.harvard.edu.

Author Contributions

Chen Lossos- designed and performed experiments, analyzed data, wrote the manuscript
Yunpeng Liu- designed and performed experiments, analyzed data, wrote the manuscript
Kellie E. Kolb- designed and performed experiments, analyzed data, wrote the manuscript
Amanda L. Christie- designed and performed experiments and analyzed data
Alexandria Van Scoyk- performed experiments
Sanjay M. Prakadan- designed and performed experiments, analyzed data
Kay Shigemori- performed experiments
Kristen E. Stevenson- analyzed data, wrote the manuscript
Sara Morrow- performed experiments
Olivia D. Plana- performed experiments
Cameron Fraser- performed experiments, analyzed data, wrote the manuscript
Kristen L. Jones- performed experiments
Huiyun Liu- performed experiments
Christian C. Pallasch- provided reagents
Rebecca Modiste- performed experiments, analyzed data
Quang-De Nguyen- performed experiments, analyzed data, wrote the manuscript
Jeffrey W. Craig- performed experiments, analyzed data
Elizabeth A. Morgan- designed and performed experiments, analyzed data, wrote the manuscript
Francisco Vega- designed and performed experiments, analyzed data, wrote the manuscript
Jon C. Aster- designed experiments, analyzed data, wrote the manuscript
Kristopher A. Sarosiek- designed experiments, analyzed data, wrote the manuscript
Alex K. Shalek- designed experiments, analyzed data, wrote the manuscript
Michael T. Hemann- designed experiments, analyzed data, wrote the manuscript
David M. Weinstock- conceived the study, designed experiments, analyzed data, wrote the manuscript

Declarations of Interest: The authors declare no relevant conflicts of interest.

[7]Laboratory of Systems Pharmacology, Harvard Program in Therapeutics Science, Department of Systems Biology, Harvard Medical School. Boston, MA 02115.

[8]Department of Internal Medicine, University Hospital of Cologne, Cologne, Germany.

[9]Lurie Family Imaging Center, Center for Biomedical Imaging in Oncology, Dana-Farber Cancer Institute, Boston, MA 02215, USA.

[10]Department of Pathology, Brigham and Women's Hospital, Harvard Medical School, Boston, MA, 02115, USA.

[11]Division of Hematopathology, Department of Pathology and Laboratory Medicine, University of Miami/Sylvester Comprehensive Cancer Center, Miami, FL, USA; Division of Hematology-Oncology, Department of Medicine, Sylvester Comprehensive Cancer Center, University of Miami, Miami, FL, USA

Abstract

The extraordinary activity of high-dose cyclophosphamide against some high-grade lymphomas was described nearly 60 years ago. Here we address mechanisms that mediate cyclophosphamide activity in *bona fide* human double-hit lymphoma. We show that antibody resistance within the bone marrow (BM) is not present upon early engraftment but develops during lymphoma progression. This resistance required a high tumor: macrophage ratio, was recapitulated in spleen by partial macrophage depletion and was overcome by multiple, high-dose alkylating agents. Cyclophosphamide induced ER-stress in BM-resident lymphoma cells *in vivo* that resulted in ATF4-mediated paracrine secretion of VEGF-A, massive macrophage infiltration and clearance of alemtuzumab-opsonized cells. BM macrophages isolated after cyclophosphamide treatment had increased phagocytic capacity that was reversed by VEGF-A blockade or SYK inhibition. Single-cell RNA sequencing of these macrophages identified a "super-phagocytic" subset that expressed CD36/FcgRIV. Together, these findings define a novel mechanism through which high-dose alkylating agents promote macrophage-dependent lymphoma clearance.

Introduction

The alkylating agent cyclophosphamide (CTX) first became available in 1959 (1,2). Soon thereafter, CTX was noted to have remarkable single-agent activity in the treatment of endemic Burkitt lymphoma. In fact, a fraction of high-grade lymphomas could be cured with a single dose of CTX (3,4), a response that is wholly unique among aggressive cancers. The mechanisms through which CTX exerts this profound efficacy have remained largely unclear.

Cell lines developed from high-grade lymphomas like Burkitt lymphoma have similar sensitivities to alkylating agents as they do to topoisomerase II poisons (e.g. doxorubicin, etoposide), vinca alkaloids and other chemotherapies (5-7). Thus, there does not appear to be a lymphoma cell-autonomous sensitivity specific to alkylating agents. This leaves the remarkable *in vivo* activity of high-dose CTX unexplained, but one possibility is that it involves the lymphoma microenvironment. High doses of CTX are extremely lymphodepleting (8,9), so it is unlikely that adaptive immunity plays a large role in its

activity. In contrast, macrophages are largely resistant to chemotherapy, including high-doses of alkylating agents like CTX. Chemotherapies such as doxorubicin and cyclophosphamide can be “immunogenic” and increase macrophage-mediated clearance of tumor cells (10,11). Of note, BL and other high-grade lymphomas with *MYC* rearrangements commonly have a “starry sky” appearance under the microscope due to infiltration of the microenvironment by lymphoma-associated macrophages (12,13).

Monoclonal antibodies like rituximab and alemtuzumab (Alem), which bind to CD20 and CD52, respectively, are widely utilized in the treatment of lymphomas. These antibodies function through various mechanisms, including antibody-dependent cellular phagocytosis (ADCP) by macrophages, antibody-dependent cellular cytotoxicity (ADCC) by NK cells and complement-dependent cytotoxicity (CDC) (14-16). Both rituximab and Alem have reduced activity at sites of bulky disease (17,18), suggesting at least two possibilities: (1) the antibodies have poor penetration into sites of bulky disease and/or (2) bulky disease represents a later stage of disease progression, in which the lymphoma microenvironment is less amenable to antibody-dependent lymphoma killing.

We previously treated NOD.SCID.*IL2Rγ*$^{-/-}$ (NSG) mice transplanted with a humanized model of CD20^{low}CD52^{high} B-cell leukemia/lymphoma (19) with Alem, which led to near elimination of tumor in blood and spleen but not bone marrow (BM). Resistance in the BM was successfully overcome by treatment with high-dose CTX (20). To more faithfully model human aggressive lymphomas, we have established patient-derived xenografts (PDXs) of double-hit lymphoma (DHL). DHL is a highly aggressive subtype of B-cell lymphoma that is frequently resistant to rituximab-containing immunochemotherapy like R-CHOP, commonly involves the bone marrow (21,22) and has a very poor prognosis (23,24). Novel treatments for DHL are a recognized area of clinical need. Approximately 75% of DHLs highly express CD52, suggesting Alem may have efficacy in this disease (21). Of note, Alem has been used extensively to treat chronic lymphocytic leukemia and other lymphoid malignancies involving the bone marrow, especially in the rituximab-refractory setting (25).

Important biological questions from our previous work remain unanswered. First, do the effects of high-dose CTX extend to *bona fide* human lymphomas? Second, do other alkylating agents recapitulate the effects observed with high-dose CTX? Third, what components of bone marrow remodeling that occur during disease progression drive therapeutic resistance? Fourth, are macrophages required for CTX-mediated killing in the BM microenvironment? Fifth, how does CTX induce crosstalk *in vivo* between lymphoma cells and macrophages? Finally, does the *in vivo* crosstalk modify the transcriptional and phenotypic states of macrophages to promote phagocytosis? Here we utilize *in vivo* models of human DHL to specifically address mechanisms underlying the notable activity of high-dose cyclophosphamide described in patients with aggressive lymphomas.

Results

Alkylating agents overcome therapeutic resistance of human lymphoma cells in the BM. DFBL-20954 and DFBL-69487 are DHL PDXs that harbor translocations of both *MYC* and *BCL2* (Supplementary Figure 1A) (26). Both DFBL-20954 and DFBL-69487 are CD52^{high}/

CD20$^{low/negative}$ (Figure 1A, Supplementary Figure 1B), consistent with a subset of DHLs (27,28) and observed with acquired resistance to rituximab-based therapy (29). In fact, both PDXs were established from biopsies obtained after treatment failure with R-CHOP, which includes rituximab and a lower dose of CTX (750mg/m^2).

NSG mice were xenografted with these lymphomas and monitored until they had >2% peripheral blood hCD19$^+$CD45$^+$ cells (approximately days 21 and 35 post injection for DFBL-20954 and DFBL-69487, respectively). Mice were randomized to receive vehicle, CTX (100mg/kg) on day 0, Alem (5mg/kg/day) on days 0 and 1, or the combination (20). Mice treated with Alem and sacrificed on day 8 had near complete elimination of lymphoma cells in the peripheral blood and spleen compared to vehicle-treated mice, but Alem had almost no effect in the BM (Figure 1B, 1C, Supplementary Figure 2A). *In vitro* exposure to Alem for 48 hours had no effect on the viability of either PDX (Supplementary Figure 2B), suggesting that Alem efficacy is dependent on *in vivo* factors.

Lower doses of CTX (25mg/kg or 50mg/kg) had markedly reduced effects on BM DHL cells compared to CTX 100mg/kg (Supplementary Figure 2C). Consistent with low expression of CD20 on both DHLs, rituximab failed to synergize with high-dose CTX in eliminating splenic and BM disease (Supplementary Figure 2D). Moreover, high-dose CTX and Alem induced significantly greater BM tumor clearance than an R-CHOP regimen (30,31). Rituximab failed to induce apoptosis or phagocytosis by bone marrow derived macrophages (BMDMs) *in vitro* (Supplementary Figure 2E, 2F).

Treatment with the maximum-tolerated dose of doxorubicin (Dox) also reduced splenic but not BM lymphoma and was not synergistic with Alem (Figure 1B). Because Dox induces DNA double-strand breaks (DSBs) that lead to apoptosis, we hypothesized that lymphoma cells resident within the BM may be less susceptible to DNA damage-induced apoptosis (*i.e.,* less “primed”) than those in the spleen. We used BH3 profiling (32) to assess apoptotic priming of lymphoma cells from the two compartments, which involves adding pro-apoptotic peptides to cells and quantifying the extent to which they induce mitochondrial permeabilization. Surprisingly, BM lymphoma cells were more primed to undergo apoptosis than spleen lymphoma cells (Supplementary Figure 2G). Thus, the resistance of BM lymphoma cells to Dox involves non-lymphoma cell-autonomous effects within the BM microenvironment.

In contrast to Dox, CTX monotherapy reduced lymphoma burden by approximately 10-fold in the BM and was highly synergistic (160-fold in DFBL-02954, 88-fold in DFBL-69487) with Alem (Figure 1B). Importantly, *in vivo* treatment with Dox or CTX induced similar levels of DNA DSBs (Supplementary Figure 2H) and apoptotic priming (Supplementary Figure 2I) within BM lymphoma cells. Thus, the unique efficacy of CTX is unlikely to depend solely on DNA damage or induction of lymphoma apoptosis. Treatment with CTX resulted in significantly increased survival compared with vehicle- or Alem-treated mice ($p<0.001$, Figure 1D). Mice receiving the combination of CTX plus Alem had significantly increased survival compared to either agent alone (both comparisons $p<0.001$, Figure 1D), consistent with *in vivo* synergy.

We next asked whether other alkylating agents could recapitulate the effects of CTX on lymphoma cells in the BM. Like CTX, the nitrogen mustard ifosfamide and the alkyl sulfonate busulfan each reduced lymphoma burden in the BM of treated mice and were synergistic with Alem (Figure 1E). The BCL2/BCL-xL inhibitor navitoclax reduced BM lymphoma percentage by ~20% ($p=0.0011$ versus PBS) but, in contrast with the alkylating agents, did not induce synergistic effects with Alem (Figure 1E). Thus, synergy with Alem is unlikely to depend solely on the induction of apoptosis.

Lymphoma: effector ratio determines the response to Alem. To address the mechanisms of Alem resistance in the BM, we first asked whether the burden of disease affected therapeutic efficacy. We injected DFBL-20954 cells into mice and initiated Alem treatment after 8, 12 or 16 days. Treatment with Alem at any of the time points led to marked reductions in spleen lymphoma cells 3 days after treatment initiation (e.g. at day 11 after treatment on day 8) (Figure 2A). In contrast, Alem reduced BM lymphoma cells when given on days 8 or 12 but not when given on day 16 (Figure 2A) or 21 (Figure 1C). Thus, resistance to Alem in the BM is associated with more extensive lymphoma involvement. Alem labeling of lymphoma cells was similar in the BM and spleen of mice treated 21 days after xenografting (Figure 2B). Moreover, Alem binding of lymphoma cells was detected in the BM up to 5 days after dosing (Supplementary Figure 3A), consistent with past reports of Alem *in vivo* half-life (33,34). Together, these data suggest that resistance to Alem within the BM is not due to inadequate antibody penetration.

We next asked whether resistance was driven by differences in macrophage involvement between the BM and spleen. We treated lymphoma-engrafted mice with clodronate at a dose that almost completely depleted macrophages from the spleen and BM (Supplementary Figure 3B). We dosed Alem on day 12 after xenografting, a timepoint when Alem leads to approximately 50% depletion of BM lymphoma cells 3 days later (Figure 2A). Treatment with clodronate on day 10 (2 days prior to Alem) completely abrogated Alem effects in both the spleen and BM (Figure 2C). Thus, macrophages are required for Alem-mediated lymphoma clearance. Pretreatment with clodronate also largely reversed the effects of CTX (alone or with Alem) on lymphoma involvement in the BM (Figure 2D), indicating that macrophages contribute to CTX-induced lymphoma clearance.

We next asked whether lymphoma engraftment within the BM reduces the phagocytic capacity of macrophages within that compartment. We sorted primary $CD11b^{+}F4/80^{+}$ monocytes/macrophages from BM of either unengrafted NSG mice or NSG mice bearing the lymphoma xenografts. We then assayed *ex vivo* phagocytosis of BM lymphoma cells collected from untreated mice. *Ex vivo* phagocytosis did not differ significantly between macrophages from BM of unengrafted NSG mice and from NSG mice engrafted with lymphoma on day 21, either in the presence or the absence of Alem (Figure 2E). The same results were observed using the BL cell line Raji to which the macrophages were not previously exposed (Figure 2E). These data suggest that “tolerization” of macrophages induced by lymphoma cells was not a driver of BM resistance.

We next asked whether BM resistance to Alem at day 21 was due to an inherently lower phagocytic capacity of BM macrophages to phagocytose lymphoma cells compared to

spleen macrophages. To test this, we sorted splenic and BM macrophages from unengrafted NSG mice or mice engrafted with lymphoma on day 21 and assayed their *ex vivo* capacity to phagocytose BM lymphoma cells. Again, there were no differences in the phagocytic capacity of splenic and BM macrophages *ex vivo* (Figure 2F).

We noted that at day 21 after xenografting, mice had 2-fold (model 20954; Figure 2G) or 8-fold (model 69487; Supplementary Figure 3C) higher lymphoma: macrophage (*i.e.,* target: effector) ratios in the BM compared to the spleen. To more rigorously assess whether the lymphoma: macrophage ratio was a driver of antibody resistance, we gave a reduced dose of clodronate to lymphoma-engrafted mice to partially deplete macrophages and thereby establish a lymphoma: macrophage ratio in the spleen like that observed in the BM. At a dose of clodronate that reduced splenic macrophages by ~75% (Supplementary Figure 3D), the effects of Alem on splenic lymphoma were almost completely reversed (Figure 2H). Together, these data suggest that the higher lymphoma: macrophage ratio that occurs upon extensive BM lymphoma involvement is the primary driver of Alem resistance.

Treatment with CTX but not Dox significantly reduced the BM lymphoma: macrophage ratio in both models (Figure 2G, Supplementary Figure 3C). This was associated with a striking increase in the fractional abundance of macrophages in the BM 8 days after treatment with CTX but not with Dox (Figure 2I). Because macrophages can adhere to stromal elements within the BM microenvironment and be difficult to remove by mechanical flushing, flow cytometric quantification may underestimate macrophage involvement. Thus, we stained femurs from treated mice for the macrophage marker F4/80, which showed that the BM space of CTX-treated mice was packed with macrophages (Figure 2J). Fewer than 5% of macrophages within the BM of CTX-treated mice were in S or G2/M phase of the cell cycle (Supplementary Figure 3E), suggesting that these cells did not proliferate within the BM but instead trafficked there after CTX treatment.

Reduced phagocytic proneness of BM lymphoma cells is reversed by cyclophosphamide. Having established that lymphoma: macrophage ratios differ within the BM and spleen at late timepoints, we next asked whether the altered ratio could be due to BM lymphoma cells being less prone to macrophage phagocytosis. We isolated viable (Annexin V-negative) lymphoma cells from the spleen and BM 21 days after xenografting and assessed their capacity to be phagocytosed by BMDMs from unengrafted NSG mice *ex vivo* (see Methods). More splenic lymphoma cells were phagocytosed compared to BM lymphoma cells, both in the presence and absence of Alem (Figure 3A). In addition, more BM lymphoma cells from mice treated with CTX were phagocytosed compared to lymphoma cells from mice treated with vehicle or Dox (Figure 3A).

To address the mechanisms underlying reduced macrophage phagocytosis of BM lymphoma cells, we quantified levels of factors known to affect phagocytosis or antibody efficacy at day 21 after xenografting. We identified increased levels of the anti-phagocytic factors prostaglandin E2 (PGE2) (35), CD32 (36) and galectin-1 (37) in BM lymphoma cells compared to spleen lymphoma cells (Figure 3B). At the same time, the pro-phagocytic molecule VISTA (38) was decreased in BM lymphoma cells compared to spleen lymphoma cells (Figure 3B). Addition of recombinant PGE2 (2 ng/ml) inhibited macrophage

phagocytosis of BM lymphoma cells *in vitro* in both the presence and absence of Alem (Figure 3C, Supplementary Figure 4A). Similarly, the addition of recombinant galectin-1 (500 ng/ml) inhibited antibody-mediated phagocytosis of lymphoma cells by BMDMs *ex vivo*, which was reversed by the galectin-1 inhibitor lactose (Figure 3D).

We hypothesized that CTX augments lymphoma cell phagocytic proneness by shifting the balance of pro- and anti-phagocytic factors. Indeed, treatment with CTX lowered surface levels of the anti-phagocytic molecule CD47 and increased surface expression of both VISTA and calreticulin (Figure 3E, Supplementary Figure 4B). In contrast, CTX had no effect on the levels of surface CD52 (Figure 3E). Total levels of PGE2 and galectin-1 were reduced in lymphoma cells from the BM of CTX-treated mice compared to vehicle- or Dox-treated mice (Figure 3E, Supplementary Figure 4B). These observations suggest that high-dose CTX increases the susceptibility of human lymphoma cells to be phagocytosed by macrophages at least in part through remodeling of effector: target interactions.

To further confirm this model, we generated conditioned media by isolating BM lymphoma cells from mice 21 days after engraftment and 6 hours after *in vivo* treatment with PBS, Dox or CTX. Equal numbers of lymphoma cells from each condition were washed and then incubated *ex vivo* for 24 hours. The conditioned media was then applied to a co-culture of NSG BMDMs with lymphoma cells in the presence or absence of Alem. Conditioned media generated from CTX-treated lymphoma cells increased phagocytosis in the presence of Alem (Figure 4A), confirming that humoral factors induced by CTX treatment can promote ADCP. Human cytokine profiling of whole BM identified increases in both VEGF-A and IL-16 from mice treated with CTX, ifosfamide or busulfan (Figure 4B and Supplementary Figure 4C, D). Increased levels of human VEGF-A were also observed in the conditioned media from mice treated with CTX (Supplementary Figure 4E). Consistent with the role of IL-16 in specifically recruiting CD4+ macrophages (39), we observed a higher fraction of macrophages that were $CD4^+$ in the BM of CTX-treated but not Dox-treated mice (Supplementary Figure 4F).

Addition of recombinant human VEGF-A increased *in vitro* phagocytosis of Alem-treated lymphoma cells by BMDMs (Figure 4C). Addition of the anti-human VEGF-A antibody bevacizumab completely blocked the pro-phagocytic effect of conditioned media collected from the BM of lymphoma-engrafted mice treated with CTX (Figure 4D). Higher doses of recombinant galectin-1 (1 ¼g/ml) and PGE-2 (5ng/ml) were needed to inhibit BMDM phagocytosis upon incubation with CTX-conditioned media (compared to control media) (Figure 4D), consistent with reductions in their concentrations in the CTX-conditioned media (Figure 3E). Treatment of lymphoma-engrafted mice with bevacizumab decreased the efficacy of CTX plus Alem *in vivo*, confirming that VEGF-A secreted by human lymphoma cells in the BM is necessary for maximal synergy (Figure 4E).

Previous reports have demonstrated that VEGF-A increases phosphorylation of the SYK kinase in macrophages, which is also downstream of Fc receptors and known to be essential for antibody-mediated phagocytosis (40). We confirmed that VEGF-A increased SYK phosphorylation in BMDMs ($p < 0.05$, Supplementary Figure 4G). VEGF-A also enhanced SYK phosphorylation over levels induced by antibody-Fc cross-linking ($p<0.05$,

Supplementary Figure 4G). Addition of the SYK inhibitor BAY61–3606 blocked SYK phosphorylation that was induced by VEGF-A and crosslinking (Supplementary Figure 4G) and abrogated the ability of VEGF-A to enhance macrophage phagocytosis of Alem-treated lymphoma cells *in vitro* (Figure 4F). Taken together these studies suggest that VEGF-A enhances macrophage phagocytosis through SYK activation and that this effect is reversed by a SYK inhibitor.

CTX induces a secretory response within BM lymphoma cells through ER stress. We next sought to understand what promotes CTX-mediated VEGF-A production. We performed RNA-Seq analysis of purified lymphoma cells from the spleen and BM collected 16 hours after vehicle, Dox or CTX treatment. VEGF-A mRNA expression was increased after CTX but not Dox treatment in both spleen and BM cells (Supplementary Table 1).

We performed gene-set enrichment analyses (GSEA) and focused on signatures that were specifically enriched in lymphoma cells from both the spleen and BM of CTX-treated mice compared to PBS- or Dox-treated mice. We noted multiple signatures corresponding to NF-kB activation, amino acid deprivation and ER stress (Figure 5A, Supplementary Table 2). Amino acid deprivation is known to activate the ER stress executioner protein ATF4 (41). ER stress can also drive NF-kB activation and VEGF-A secretion in multiple contexts (42-45). ATF4 and spliced XBP-1 can both induce VEGF-A transcription (43,46,47) and were increased in BM lymphoma cells from CTX-treated mice compared to vehicle- or Dox-treated mice (Figure 5B, Supplementary Figure 5A, B).

Ex vivo exposure of BM lymphoma cells to either of the ER stress-inducing agents thapsigargin or tunicamycin was sufficient to increase production and secretion of VEGF-A (Figure 5C, Supplementary Figure 5C). Of note, a lower dose of CTX (50 mg/kg) given *in vivo* was unable to induce ATF4 protein or secretion of VEGF-A in BM lymphoma cells but did partially induce spliced XBP-1 (Figure 5D, 5E). ChIP-qPCR of purified BM lymphoma cells demonstrated significantly increased ATF4 recruitment to exon 1 of *VEGFA* (47) after CTX treatment but not to a negative control region (Figure 5F). We also observed ATF4 recruitment to *VEGFA* following Dox treatment in the DFBL-69487 model but to a lesser extent than following CTX treatment. Together these observations suggest that high-dose CTX induces ER stress within BM lymphoma cells that involves upregulation of ATF4, which drives VEGF-A production and secretion.

CTX treatment of lymphoma cells induces a pro-phagocytic transcriptional response in BM macrophages that synergizes with Alem. Next, we addressed the effects of CTX treatment on macrophages within the BM lymphoma environment. We isolated BM and splenic macrophages from lymphoma-bearing mice 48 hours after treatment with vehicle, Dox or CTX and assayed their capacity to phagocytose Alem-coated lymphoma cells. Macrophages were also isolated from unengrafted NSG mice after treatment with vehicle or CTX. Phagocytosis of Raji lymphoma cells was similar between macrophages from unengrafted mice treated with vehicle or CTX (Figure 6A, Supplementary Figure 6A). In contrast, phagocytosis was markedly increased by macrophages from lymphoma-bearing mice after treatment with CTX compared to vehicle (Figure 6A, Supplementary Figure 6A). Importantly, this effect was not due to nonspecific cell death as Dox treatment, which

induces similar levels of cell death as CTX treatment in the spleen (Figure 1B), did not increase the phagocytic capacity of splenic macrophages from engrafted mice for lymphoma cells (Figure 6A, Supplementary Figure 6A). This effect was not specific to Alem, as macrophages from tumor-bearing, CTX-treated mice also had increased uptake of rituximab-coated Raji cells (Supplementary Figure 6B). High doses of CTX (100mg/kg) were required to enhance phagocytosis of cells coated with either antibody (Supplementary Figure 6B). In addition, *ex vivo* pre-treatment of macrophages with Dox, mafosfamide (a CTX analog that is active *in vitro*) or ifosfamide failed to increase phagocytosis (Supplementary Figure 6C). These observations indicate that *in vivo* treatment with CTX in the presence of lymphoma is required to enhance the phagocytic capacity of macrophages.

To define transcriptional correlates for these phenotypes, we sorted primary BM macrophages 48 hours after *in vivo* treatment of engrafted mice with vehicle, Alem, Dox, CTX or CTX plus Alem and performed RNA-seq (Supplementary Table 3). The same population was also sorted from the BM of unengrafted NSG mice treated with either vehicle or CTX. Macrophages are commonly categorized by transcriptional signatures into M0 (undifferentiated), M1 (anti-tumor) and M2 (tumor-promoting) subtypes. We performed multi-dimensional scaling (MDS) analysis using existing signatures from *in vitro*-differentiated M0, M1 and M2 macrophages as reference groups (48). Macrophages from unengrafted NSG mice treated with vehicle clustered farthest from any of the three reference groups. Upon engraftment of lymphoma cells, the macrophages shifted to a more M2-like signature (Figure 6B) that was unaffected by *in vivo* treatment with Alem or Dox. Treatment of either unengrafted mice or lymphoma-engrafted mice with CTX (or the combination of CTX plus Alem) generated a new transcriptional cluster (Figure 6B) that was distinct by differential gene expression (Supplementary Figure 6D, Supplementary Table 4). This new cluster was closer to M2 by MDS but did not differ in surface expression of MHC class II and CD206 compared to BM macrophages from vehicle-, Dox- or Alem-treated mice (Supplementary Figure 6E).

Bulk RNAseq like the experiments outlined above cannot distinguish whether CTX induces a heterogenous mixture of different macrophage types. Therefore, we also performed Smart-Seq2 single-cell RNA-seq (scRNAseq) (49) on BM macrophages collected 48 hours after treatment of mice engrafted with either lymphoma and treated with vehicle, Dox or CTX, or unengrafted mice treated with vehicle or CTX. After filtering for quality (see Supplementary Methods), we performed dimensionality reduction (PCA) and graph-based clustering (shared nearest neighbors, snn) on the unified cells-by-genes expression matrix and visualized our results via t-distributed stochastic neighbor embedding (t-SNE). Our unbiased analysis identified 6 unique macrophage clusters (Figure 6C). Notably, there was similar representation within each macrophage cluster between the two models, with the exception of C5, which was predominately comprised of macrophages from mice engrafted with DFBL-69487 and was dominated by genes associated with eosinophils (Supplementary Table). Importantly, two clusters (C2 and C4, respectively, Supplementary Figure 6F, Supplementary Table 5) were enriched for macrophages from lymphoma-bearing mice treated with CTX (Figure 6C, $p = 3.7 \times 10^{-8}$ for C2, $p = 1.7 \times 10^{-9}$ for C4, Fisher's Exact Test, Bonferroni corrected for 25 tests). Cells from clusters 2 and 4 were enriched for

expression of genes known to be important in macrophage-mediated phagocytosis, including CD36 and PPARγ (50,51) (Supplementary Tables 5 and 6).

We noted a striking increase in the expression of Fcgr1, the high-affinity human IgG receptor, in cluster 2 macrophages (Figure 6D; $p = 5.28 \times 10^{-15}$, Bonferroni corrected for 24 comparisons; effect size cohen's d = 1.04). At the same time, cluster 4 had markedly higher expression of Fcgr4 (Figure 6D; $p = 5.28 \times 10^{-15}$, Bonferroni corrected for 24 tests, effect size Cohen's d = 2.54). Flow cytometric analysis of macrophages from the spleen and BM confirmed increases in the overall expression of activating Fc receptors (Fcgr1, Fcgr3 and Fcgr4) and decreased expression of the inhibitory Fcgr2B receptor on the surface of lymphoma cells from engrafted mice treated with CTX (Figure 6E). Interestingly, doxorubicin treatment of lymphoma-engrafted mice increased Fcgr2B surface expression on both splenic and BM macrophages (Figure 6E). Ingenuity Pathway Analysis (IPA) of C2 and C4 cells showed enrichment of genes involved in Fc-receptor mediated phagocytosis and phagosome formation and maturation (Supplementary Tables 5 and 6).

For both lymphomas, we noted that cluster 4 macrophages comprised approximately 20–25% of BM macrophages after CTX treatment. Thus, we hypothesized that cluster 4 specifically defines macrophages with "super-phagocytic" capacity for Alem-coated cells. To address this, we flow-sorted macrophages from the BM of lymphoma-bearing mice treated with vehicle or CTX based on FcgRIV and CD36 (Figure 6F). As expected, CTX-treated mice had an increased percentage of BM $FcgRIV^{high}/CD36^{+}$ macrophages (Figure 6F). Phagocytosis of Alem-opsonized lymphoma cells was enhanced among macrophages from this population compared to $CD36^{low/negative}$ or $FcgRIV^{low}$ cells (Figure 6G). Finally, IPA upstream pathway analysis showed VEGF as a regulator of the C4 signature (Supplementary Table 7). Thus, the cluster 4 signature defines a unique macrophage state that is inducted specifically by CTX in the presence of lymphoma cells and has enhanced ability to phagocytose antibody-coated lymphoma cells.

Discussion

Treatment-resistant niches pose a challenge to effective cancer therapy. The bone marrow is a frequent site of minimal residual disease in both hematologic and non-hematologic tumors, suggesting compartment-specific mechanisms of resistance (52,53). Using orthotopic models of aggressive human lymphoma, we recapitulated resistance to both antibody and doxorubicin therapy within the BM and defined resistance mechanisms through comparisons with the spleen, a site of consistent drug activity.

Previous analyses of antibody resistance in lymphomas have identified several lymphoma cell-autonomous mechanisms, including the loss of target antigen and changes in the expression of pro- and anti-phagocytic factors (29,54,55). In our models, Alem resistance was achieved through BM remodeling that involved high lymphoma: macrophage ratios at later stages of engraftment. We recapitulated antibody resistance within the spleen solely by partial depletion of macrophages. Although clodronate may have unexpected effects on cells other than macrophages, these findings strongly suggest that lymphoma: macrophage ratio is a primary determinant of antibody response within our models. Late engraftment was

associated with higher levels of CD32, galectin-1 and PGE2. Each of these factors can decrease antibody-mediated lymphoma clearance by macrophages (35,37), which we confirmed for both galectin-1 and PGE2. It remains poorly understood how the BM microenvironment interacts with lymphoma cells to modulate the expression of these factors as well as the extent to which other tumor types develop resistance within the BM through these same factors.

Treatment with high-dose CTX (but not a dose closer to that in R-CHOP) overcame antibody resistance within the BM, leading to marked synergy with alemtuzumab. This suggests that diseases involving the BM that are known to be responsive to alemtuzumab, such as chronic lymphocytic leukemia, may benefit from combinations with high-dose CTX. At the same time, other antibodies beside alemtuzumab presumably also synergize with high-dose CTX if there is adequate expression of the target antigen. In fact, other studies have reported that CTX can overcome resistance to rituximab or a carcinoma-specific antibody in an Fc receptor-dependent manner (20,56). Notably, high doses of other alkylating agents also induced synergy within the BM to CTX but other classes of cytotoxic chemotherapy or navitoclax, which directly induces apoptosis, did not. Thus, the activity of high-dose alkylating agents does not solely involve either clastogenesis or apoptotic cell death. Instead, we show that CTX treatment of engrafted mice leads to a remarkable infiltration of macrophages within the BM, an altered balance of pro- and anti-phagocytic markers and secretion of pro-phagocytic cytokines.

A central unanswered question is whether the findings in the BM of our xenografts are applicable to sites with high tumor: effector cell ratios in humans. To this end, treatment with high dose CTX may be an effective strategy for overcoming sites of bulky disease, which are known to be relatively refractory to monoclonal antibodies (18). Ultimately, paired biopsies from bulky and non-bulky sites of lymphoma will be needed to clarify whether the former have higher tumor: effector cell ratios and whether those ratios correlate with differential response to monoclonal antibodies.

The anti-neoplastic activity of alkylating agents has classically been linked to the direct induction of DNA adducts that result in single- and double-strand DNA breaks (57). However, from the first description of these compounds it has been clear that they can alkylate a variety of proteins, lipids and other molecules (58). Based on changes in gene expression induced by CTX treatment, we identified ER stress within DHL cells after treatment with high-dose (but not lower-dose) CTX. The mechanism through which high-dose CTX induces this ER stress is unclear but it could involve protein misfolding, which is known to induce ER stress through the unfolded protein response (42). It is possible that chemical modifications of proteins and other non-DNA targets reach a threshold only with higher concentrations of alkylating agents and their metabolites. This would help explain why high-dose CTX is required to induce ER stress. It also remains unclear to what extent ER stress is sufficient to drive the complex interactions between lymphoma cells and the BM microenvironment after CTX treatment.

ER stress within BM lymphoma cells after CTX treatment led to upregulation of ATF4, which can bind *VEGF-A* regulatory regions. The associated secretory response, *in concert*

with the more pro-phagocytic balance of lymphoma surface signals, then promotes macrophage phagocytosis. The VEGF-A response is required as either bevacizumab or SYK inhibition reversed the increased phagocytosis induced by CTX. These findings provide multiple notes of caution. Agents included within chemotherapy regimens such as glucocorticoids may suppress the activity of macrophages and thereby antagonize high-dose alkylating agents. Similarly, trials of bevacizumab or SYK inhibition, which both suppress macrophage-mediated clearance of lymphoma cells in our experiments, are currently underway in combinations with chemoimmunotherapy. It is possible that these agents will have direct cytotoxic effects on lymphoma cells but antagonize macrophage responses. Finally, studies using cell lines to identify interactions between therapeutic agents will not capture antagonisms that depend on microenvironmental and immune cell interactions.

Using single-cell RNA-seq, we show that a diverse set of transcriptionally-unique macrophage clusters are present within lymphoma-engrafted BM and this biology is markedly altered by CTX. The classical distinctions between M0, M1 and M2 macrophages that were defined based on *in vitro* studies fail to capture this diversity *in vivo* or the effects from CTX. Most notably, CTX treatment leads to marked enrichment of two unique macrophage subgroups, designated here as C2 and C4. C4 macrophages had high expression of Fcgr4 and CD36 transcripts. Sorted macrophages with surface $Fcgr4^{high}/CD36^{+}$ immunophenotype had “super-phagocytic” capacity when exposed to BM lymphoma cells *ex vivo*, suggesting that these are the primary effectors that mediate the activity of single-agent CTX. In contrast, C2 macrophages were characterized by increased expression of Fcgr1, the high affinity Fc receptor that likely mediates most ADCP (59). Thus, one possibility is that C4 macrophages are capable of clearing lymphoma cells after CTX treatment alone while C2 macrophage orchestrate most of the synergistic effects observed with the addition of alemtuzumab. It is also worth noting that doxorubicin treatment increased surface expression of the inhibitory Fcgr2B on both splenic and BM macrophages (Figure 6E), suggesting that combining doxorubicin with high-dose alkylating agents could suppress ADCP.

We opened a clinical trial of alemtuzumab plus cyclophosphamide in patients with CD52-positive lymphomas (https://clinicaltrials.gov/ct2/show/NCT03132584). Treatment with this dose of CTX requires hospitalization and patients receive alemtuzumab without steroids. Thus, the toxicity and cost are significant. It will be important to determine whether other agents that induce aspects of the “super-phagocytic” response we describe here are equally efficacious in model systems. These could include blockers of CD47-SIRPα interaction, direct inducers of ER stress or agents that directly block mediators of antibody resistance within the BM such as non-steroidal anti-inflammatory drugs to suppress PGE2 production. Strategies that avoid high doses of alkylating agents may have the additional advantage of maintaining aspects of adaptive immunity important for long-term tumor control and could be applied across multiple cancer types.

In summary, we describe a mechanism to sensitize treatment-refractory malignancies to immunotherapy that may be particularly relevant to tumors or specific tumor compartments that do not undergo rapid apoptosis in response to therapy. Current drug regimens include

agents that may antagonize this process and thus subvert the efficacy of immune-directed therapies.

Methods

Mouse Models and Therapeutics

DFBL-20954 and DFBL-69487 are available from the Public Repository of Xenografts (PRoXe) (26). 6–8-week old NSG mice (Jackson labs) were injected with 10^6 tumor cells intravenously (i.v.). Mice were bled weekly and treatment was initiated when circulating disease was >2% as assessed by flow cytometry staining for hCD19 (clone HIB19, Biolegend) and hCD45 (clone HI30, Thermo Fisher). All blood samples were lysed with ammonium chloride red-blood cell buffer (VWR) prior to staining.

Clinical grade Alem (Genzyme-Sanofi) and Rituximab (Roche) were obtained dissolved in PBS at 30mg/ml and 10mg/ml, respectively, from the Dana Farber Cancer Institute Pharmacy and Cologne. Prior to administration Alemtuzumab was diluted 1:30 in PBS (10mg/kg doses) or 1:60 (5mg/kg doses) and Rituximab was diluted 1:5 and mice were dosed with 10¼l/g. Alem was administered 5mg/kg i.v. on day 0 and 5 mg/kg i.p. on day 1 of treatment to avoid tumor-lysis syndrome unless otherwise specified. Rituximab was given as a single dose at 20mg/kg i.v. on day 0 of treatment. Alem was conjugated with an APC-conjugation kit (Abcam) per the manufacturer's instructions.

Cyclophosphamide (Sigma Aldrich) was dissolved at 10mg/ml in PBS and administered i.p. on day 0 at a dose of 10ul/g of mouse body weight. For studies where cyclophosphamide was administered at 25 and 50 mg/kg, respectively, it was dissolved at 2.5 and 5 mg/ml PBS and dosed at 10ul/g of mouse body weight. Doxorubicin (Tocris Bioscience) was dissolved at 0.5mg/ml of 0.9% NaCl solution and administered i.p. at 10ul/g of mouse body weight. Ifosfamide (Sigma Aldrich) was dissolved at 20mg/ml in PBS and administered as cyclophosphamide. Busulfan (Sigma Aldrich) was dissolved in DMSO and then in PBS to generate a 2.5 mg/ml solution with 10% DMSO and dosed as 10ul/g mouse body weight for two days. Vincristine and prednisone were purchased from Sigma Aldrich and dissolved in PBS. R-CHOP dosing was given as follows: Rituximab (20mg/kg i.v., day 0), CTX (30mg/kg i.p., day 0), Doxorubicin (2.58mg/kg i.p., day 0), Vincristine (0.38mg/kg i.p., day 0) and Prednisone (5× 2mg/kg i.p., starting on day 0). All drugs were given at 10¼l/g of mouse body weight. Bevacizumab was obtained from the Beth Israel Deaconess Medical Center pharmacy dissolved at 25mg/ml in PBS and was administered at 25mg/ml at 10ul/g of mouse body weight on days −1, 0 and 1 of treatment. Navitoclax was dosed at 100mg/kg p.o. on days 0–7. All *in-vivo* experiments were conducted in accordance with Dana Farber Cancer Institute Animal Care and use Committee protocol #13–034.

Bone Marrow Derived Macrophage (BMDM) Generation

8–10-week old NSG mice were euthanized and femurs were flushed with a 27G needle and sifted through a 70 micron filter. The filtrates were Red-Blood Cell (RBC) lysed with ammonium chloride (VWR) and plated in RPMI-1640 media supplemented with 10% L929 cultured cell media (ATCC), 10% Fetal Bovine Serum (Sigma Aldrich) and 1% Pen/Strep

solution (Thermo Fisher Scientific). Media was changed every 2–3 days until day 7 when the macrophages were used for functional assays.

Cell Culture

Raji-GFP cells were a generous gift from Dr. Izidore Lossos and authenticity was validated by short tandem repeat profiling. Raji cells were maintained in RPMI-1640 media supplemented with 10% Fetal Bovine Serum (Sigma Aldrich) and 1% Pen/Strep solution (Thermo Fisher Scientific). Cells were split 1:10 every 2–3 days and checked for mycoplasma every 3 months by the Universal Mycoplasma Detection Kit (ATCC) and were last checked on 3/16/19.

Phagocytosis Assays (BMDM and In-vivo derived Macrophages)

In-vitro differentiated macrophages were generated as described above. On day 7 BMDM were plated at 1×10^5 cells per well of a 24 well plate and serum starved for 2 hours in RPMI-1640 media supplemented with 1% Pen/Strep. Target tumor cells (3:1 tumor: macrophage ratio) were labeled with CFSE (CellTrace CFSE Cell Proliferation Kit, Thermo Scientific) per the manufacturer's instructions and 30 minutes prior to co-incubation with macrophages were pre-coated with Alem, rituximab or obinutuzumab (final concentration 20¼g/mL per ml of total culture media of total plates) at 37° C. Alem coated and uncoated tumor cells were then co-incubated with macrophages for 2 hours. Following incubation, wells were washed 2X with PBS and macrophages were detached by gentle scraping in ice cold PBS. Cells were then pre-incubated with human (Human TruStain FcX, Biolegend) and murine Fc-Block (BD Biosciences) and then stained with CD11b (clone M1/M70, Biolegend) for 30 minutes at room temperature and analyzed using a Cytoflex (Beckman Coulter). Phagocytosis was measured as the fraction of GFP/CFSE positive $CD11b^+$ macrophages. All cytokines used in the assays were purchased from Peprotech and added at the indicated doses immediately following the addition of tumor cells to the macrophage co-culture. Recombinant human galectin-1 was purchased from R&D. Prostaglandin E2 and BAY61–3606 were purchased from Sigma Aldrich. Mafosfamide and lactose were purchased from Santa Cruz Biotechnology.

For phagocytosis assays using in-vivo derived macrophages, 10^6 xenograft cells were injected into 6–10-week old NSG mice. Once peripheral blood disease reached >2%, mice were treated with PBS, Dox or CTX as described above. Age controlled unengrafted mice were treated with PBS or CTX as above. Mice were euthanized and bone marrows and spleens were processed as described above. Samples were pre-treated with human Fc-block and stained with 7-AAD (Thermo Fisher Scientific), human CD19 (clone HIB19, Biolegend) murine CD11b (clone M1/M70, Biolegend) and F4/80 (clone BM8, BD Biosciences) antibodies and sorted using an LLC FACSAria (BD Biosciences). Splenic macrophages were defined as $7AAD^-CD19^-CD11b^-F4/80^+$ cells while BM macrophages were defined as $7AAD^-CD19^-CD11b^+F4/80^+$ cells. Cells were plated at 50,000 cells per well in a 96 well plate in RPMI-1640 media supplemented with 10% L929 media, 10% FBS, 1% Pen/Strep and 50mM 2-ME (Sigma Aldrich). Once cells attached and spinous processes were microscopically visible (12–16 hours after plating), macrophages were serum-starved for 2 hours and co-cultured with CFSE stained tumor cells +/− Alem as described above.

Cells were processed and analyzed as above but murine F4/80 was used to label macrophages instead of CD11b. Phagocytosis was measured as the fraction of GFP/CFSE positive $F4/80^+$ cells.

Cytokine Arrays

Mouse tibias were flushed. Whole cell suspensions or pelleted cells and the corresponding aqueous portions were incubated with NP-40 lysis buffer with Halt protease and phosphatase inhibitors 100x (Life Technologies). Thapsigargin and tunicamycin were purchased from Cell Signaling Technology and dosed at 2000 nM and 10 μg/ml, respectively. Protein amounts were quantified with a Pierce BCA Protein Assay Kit (Life technologies). Samples were diluted to contain equal amounts of total protein and were submitted to Eve Technologies (Ontario, Canada) for Human 65-plex and Murine-41 plex discovery arrays.

ELISA

Femurs were flushed and mouse depleted as described above. Protein amount was quantified using a Pierce BCA Protein Assay Kit (Life technologies). Human galectin-1 ELISA Kit was from Thermo Fischer Scientific. Prostaglandin E2 ELISA Kit was purchased from Abcam. Standard curves were generated from provided reagents and from recombinant proteins and quantified using SoftMax Pro software on a Spectromax M190 per the manufacturer's instructions.

Conditioned Media Generation

NSG mice were injected and treated as above. Six hours after treatment human tumor cells were purified using an EasySep Mouse/Human Chimera Isolation Kit (StemCell Technologies). Purified, pooled cells (10^7) were cultured in 10 ml of X-Vivo 15 media (Lonza Bioscience) for 24 hours post isolation. Cells were pelleted with centrifugation (500g) for 10 minutes and supernatant removed and applied to macrophages following serum starvation for phagocytosis assays. Thapsigargin- and tunicamycin-conditioned media was generated from 10^6 cells.

Statistics

Overall survival was determined by the Kaplan-Meier method using the log-rank test and considered signficant at the <0.05 level. Alem and CTX synergy was calculated as previously described (20). Comparisons of continuous measures between two group was made using a two-sided Welch t-test and were considered significant at the 0.05 level. Differential expression of bulk RNAseq between experimental conditions was determined using raw count data and normalization procedures within the DESeq2 package in R based on a negative binomial distribution. The false discovery rate (FDR) by Benjamini and Hochberg method was used to adjust for multiple comparions. Ordered lists determined by differential expression analysis were then used in gene set enrichment analysis (GSEA) using tools developed by the Broad Institute and FDR q-values were also reported.

Supplementary Material

Refer to Web version on PubMed Central for supplementary material.

Acknowledgements.

We thank the Dana-Farber Hematologic Neoplasia Flow Cytometry Core for their assistance. We also thank Drs. Anthony Letai, Roberto Chiarle and Andrew Lane for thoughtful discussions and experimental suggestions. Thank you to Dr. Izidore Lossos for a critical reading of the manuscript. The project described was supported by award Number T32GM007 (C.L.) from the National Institute of General Medical Sciences, the Cancer Systems Biology Consortium U54 CA217377 (A.K.S.), the Searle Scholars Program (A.K.S.), the Beckman Young Investigator Program (A.K.S.), NIH New Innovator Award 1DP2OD020839 (A.K.S.), NIH 5U24AI118672 (A.K.S.), NIH 1R33CA202820 (A.K.S.), NIH 2U19AI089992 (A.K.S.), NIH 1R01HL134539 (A.K.S.), NIH 2RM1HG006193 (A.K.S.), 2P01AI039671 (A.K.S.), the Pew-Stewart Scholars (A.K.S.), a Sloan Fellowship in Chemistry (A.K.S.), and partially by Cancer Center Support (core) Grant P30-CA14051 from the National Cancer Institute (A.K.S.), the Center for Precision Cancer Medicine at MIT (Y.L. and M.T.H.), and the Dana-Farber/Koch Institute Bridge Project (M.T.H. and D.M.W.). The content is solely the responsibility of the authors and does not necessarily represent the official views of the National Institute of General Medical Sciences or the National Institutes of Health.

References

1. George P Haemorrhagic Cystitis and Cyclophosphamide. Lancet 1963;2(7314):942.
2. Solomon J, Alexander MJ, Steinfeld JL. Cyclophosphamide. A clinical study. JAMA 1963;183:165–70. [PubMed: 13978068]
3. Burkitt D Long-term remissions following one and two-dose chemotherapy for African lymphoma. Cancer 1967;20(5):756–9. [PubMed: 6024288]
4. Clifford P, Singh S, Stjernsward J, Klein G. Long-term survival of patients with Burkitt's lymphoma: an assessment of treatment and other factors which may relate to survival. Cancer research 1967;27(12):2578–615. [PubMed: 6082297]
5. Frei E 3rd, Cucchi CA, Rosowsky A, Tantravahi R, Bernal S, Ervin TJ, et al. Alkylating agent resistance: in vitro studies with human cell lines. Proceedings of the National Academy of Sciences of the United States of America 1985;82(7):2158–62. [PubMed: 3856890]
6. Tsuruo T, Iida H, Tsukagoshi S, Sakurai Y. Potentiation of vincristine and Adriamycin effects in human hemopoietic tumor cell lines by calcium antagonists and calmodulin inhibitors. Cancer research 1983;43(5):2267–72. [PubMed: 6831450]
7. Yang W, Soares J, Greninger P, Edelman EJ, Lightfoot H, Forbes S, et al. Genomics of Drug Sensitivity in Cancer (GDSC): a resource for therapeutic biomarker discovery in cancer cells. Nucleic Acids Res 2013;41(Database issue):D955–61 doi 10.1093/nar/gks1111. [PubMed: 23180760]
8. Saida Y, Watanabe S, Tanaka T, Baba J, Sato K, Shoji S, et al. Critical Roles of Chemoresistant Effector and Regulatory T Cells in Antitumor Immunity after Lymphodepleting Chemotherapy. J Immunol 2015;195(2):726–35 doi 10.4049/jimmunol.1401468. [PubMed: 26041539]
9. Miller JS, Weisdorf DJ, Burns LJ, Slungaard A, Wagner JE, Verneris MR, et al. Lymphodepletion followed by donor lymphocyte infusion (DLI) causes significantly more acute graft-versus-host disease than DLI alone. Blood 2007;110(7):2761–3 doi 10.1182/blood-2007-05-090340. [PubMed: 17579184]
10. Wang YJ, Fletcher R, Yu J, Zhang L. Immunogenic effects of chemotherapy-induced tumor cell death. Genes Dis 2018;5(3):194–203 doi 10.1016/j.gendis.2018.05.003. [PubMed: 30320184]
11. Mantovani A, Polentarutti N, Luini W, Peri G, Spreafico F. Role of host defense merchanisms in the antitumor activity of adriamycin and daunomycin in mice. Journal of the National Cancer Institute 1979;63(1):61–6. [PubMed: 286835]
12. Ferry JA. Burkitt's lymphoma: clinicopathologic features and differential diagnosis. Oncologist 2006;11(4):375–83 doi 10.1634/theoncologist.11-4-375. [PubMed: 16614233]
13. Ford CA, Petrova S, Pound JD, Voss JJ, Melville L, Paterson M, et al. Oncogenic properties of apoptotic tumor cells in aggressive B cell lymphoma. Curr Biol 2015;25(5):577–88 doi 10.1016/j.cub.2014.12.059. [PubMed: 25702581]
14. Weiner GJ. Rituximab: mechanism of action. Semin Hematol 2010;47(2):115–23 doi 10.1053/j.seminhematol.2010.01.011. [PubMed: 20350658]

15. Leidi M, Gotti E, Bologna L, Miranda E, Rimoldi M, Sica A, et al. M2 macrophages phagocytose rituximab-opsonized leukemic targets more efficiently than m1 cells in vitro. J Immunol 2009;182(7):4415–22 doi 10.4049/jimmunol.0713732. [PubMed: 19299742]
16. Weiskopf K, Weissman IL. Macrophages are critical effectors of antibody therapies for cancer. MAbs 2015;7(2):303–10 doi 10.1080/19420862.2015.1011450. [PubMed: 25667985]
17. McLaughlin P, Grillo-Lopez AJ, Link BK, Levy R, Czuczman MS, Williams ME, et al. Rituximab chimeric anti-CD20 monoclonal antibody therapy for relapsed indolent lymphoma: half of patients respond to a four-dose treatment program. J Clin Oncol 1998;16(8):2825–33 doi 10.1200/JCO.1998.16.8.2825. [PubMed: 9704735]
18. Lundin J, Osterborg A, Brittinger G, Crowther D, Dombret H, Engert A, et al. CAMPATH-1H monoclonal antibody in therapy for previously treated low-grade non-Hodgkin's lymphomas: a phase II multicenter study. European Study Group of CAMPATH-1H Treatment in Low-Grade Non-Hodgkin's Lymphoma. J Clin Oncol 1998;16(10):3257–63 doi 10.1200/JCO.1998.16.10.3257. [PubMed: 9779699]
19. Leskov I, Pallasch CP, Drake A, Iliopoulou BP, Souza A, Shen CH, et al. Rapid generation of human B-cell lymphomas via combined expression of Myc and Bcl2 and their use as a preclinical model for biological therapies. Oncogene 2013;32(8):1066–72 doi 10.1038/onc.2012.117. [PubMed: 22484426]
20. Pallasch CP, Leskov I, Braun CJ, Vorholt D, Drake A, Soto-Feliciano YM, et al. Sensitizing protective tumor microenvironments to antibody-mediated therapy. Cell 2014;156(3):590–602 doi 10.1016/j.cell.2013.12.041. [PubMed: 24485462]
21. Craig JW, Mina MJ, Crombie JL, LaCasce AS, Weinstock DM, Pinkus GS, et al. Assessment of CD52 expression in "double-hit" and "double-expressor" lymphomas: Implications for clinical trial eligibility. PLoS One 2018;13(7):e0199708 doi 10.1371/journal.pone.0199708. [PubMed: 30020951]
22. Yao Z, Deng L, Xu-Monette ZY, Manyam GC, Jain P, Tzankov A, et al. Concordant bone marrow involvement of diffuse large B-cell lymphoma represents a distinct clinical and biological entity in the era of immunotherapy. Leukemia 2018;32(2):353–63 doi 10.1038/leu.2017.222. [PubMed: 28745330]
23. Khelfa Y, Lebowicz Y, Jamil MO. Double-Hit Large B Cell Lymphoma. Curr Oncol Rep 2017;19(11):74 doi 10.1007/s11912-017-0629-y. [PubMed: 28952038]
24. Burotto M, Berkovits A, Dunleavy K. Double hit lymphoma: from biology to therapeutic implications. Expert review of hematology 2016;9(7):669–78 doi 10.1080/17474086.2016.1182858. [PubMed: 27166590]
25. Teo EC, Chew Y, Phipps C. A review of monoclonal antibody therapies in lymphoma. Critical reviews in oncology/hematology 2016;97:72–84 doi 10.1016/j.critrevonc.2015.08.014. [PubMed: 26318093]
26. Townsend EC, Murakami MA, Christodoulou A, Christie AL, Koster J, DeSouza TA, et al. The Public Repository of Xenografts Enables Discovery and Randomized Phase II-like Trials in Mice. Cancer Cell 2016;29(4):574–86 doi 10.1016/j.ccell.2016.03.008. [PubMed: 27070704]
27. Wu D, Wood BL, Dorer R, Fromm JR. "Double-Hit" mature B-cell lymphomas show a common immunophenotype by flow cytometry that includes decreased CD20 expression. Am J Clin Pathol 2010;134(2):258–65 doi 10.1309/AJCP7YLDTJPLCE5F. [PubMed: 20660329]
28. Harrington AM, Olteanu H, Kroft SH, Eshoa C. The unique immunophenotype of double-hit lymphomas. Am J Clin Pathol 2011;135(4):649–50 doi 10.1309/AJCPL11MAHISIJBQ. [PubMed: 21411790]
29. Beers SA, French RR, Chan HT, Lim SH, Jarrett TC, Vidal RM, et al. Antigenic modulation limits the efficacy of anti-CD20 antibodies: implications for antibody selection. Blood 2010;115(25):5191–201 doi 10.1182/blood-2010-01-263533. [PubMed: 20223920]
30. Koch R, Christie AL, Crombie JL, Palmer AC, Plana D, Shigemori K, et al. Biomarker-driven strategy for MCL1 inhibition in T-cell lymphomas. Blood 2018;133:566–75 doi 10.1182/blood-2018-07-865527. [PubMed: 30498064]
31. Matthews JM, Bhatt S, Patricelli MP, Nomanbhoy TK, Jiang X, Natkunam Y, et al. Pathophysiological significance and therapeutic targeting of germinal center kinase in diffuse large

B-cell lymphoma. Blood 2016;128(2):239–48 doi 10.1182/blood-2016-02-696856. [PubMed: 27151888]

32. Ni Chonghaile T, Sarosiek KA, Vo TT, Ryan JA, Tammareddi A, Moore Vdel G, et al. Pretreatment mitochondrial priming correlates with clinical response to cytotoxic chemotherapy. Science 2011;334(6059):1129–33 doi 10.1126/science.1206727. [PubMed: 22033517]
33. Morris EC, Rebello P, Thomson KJ, Peggs KS, Kyriakou C, Goldstone AH, et al. Pharmacokinetics of alemtuzumab used for in vivo and in vitro T-cell depletion in allogeneic transplantations: relevance for early adoptive immunotherapy and infectious complications. Blood 2003;102(1):404–6 doi 10.1182/blood-2002-09-2687. [PubMed: 12623851]
34. Hu Y, Shields J, Rao S, al. e. Alemtuzumab activity and CD52 expression in human CD52 transgenic mice. Cancer Research 2007;67(9):Abstract (4133).
35. Aronoff DM, Canetti C, Peters-Golden M. Prostaglandin E2 inhibits alveolar macrophage phagocytosis through an E-prostanoid 2 receptor-mediated increase in intracellular cyclic AMP. J Immunol 2004;173(1):559–65. [PubMed: 15210817]
36. Lim SH, Vaughan AT, Ashton-Key M, Williams EL, Dixon SV, Chan HT, et al. Fc gamma receptor IIb on target B cells promotes rituximab internalization and reduces clinical efficacy. Blood 2011;118(9):2530–40 doi 10.1182/blood-2011-01-330357. [PubMed: 21768293]
37. Lykken JM, Horikawa M, Minard-Colin V, Kamata M, Miyagaki T, Poe JC, et al. Galectin-1 drives lymphoma CD20 immunotherapy resistance: validation of a preclinical system to identify resistance mechanisms. Blood 2016;127(15):1886–95 doi 10.1182/blood-2015-11-681130. [PubMed: 26888257]
38. Yoon KW, Byun S, Kwon E, Hwang SY, Chu K, Hiraki M, et al. Control of signaling-mediated clearance of apoptotic cells by the tumor suppressor p53. Science 2015;349(6247):1261669 doi 10.1126/science.1261669. [PubMed: 26228159]
39. Center DM, Cruikshank W. Modulation of lymphocyte migration by human lymphokines. I. Identification and characterization of chemoattractant activity for lymphocytes from mitogen-stimulated mononuclear cells. J Immunol 1982;128(6):2563–8. [PubMed: 7042840]
40. Yang M, Shao JH, Miao YJ, Cui W, Qi YF, Han JH, et al. Tumor cell-activated CARD9 signaling contributes to metastasis-associated macrophage polarization. Cell Death Differ 2014;21(8):1290–302 doi 10.1038/cdd.2014.45. [PubMed: 24722209]
41. Ye J, Kumanova M, Hart LS, Sloane K, Zhang H, De Panis DN, et al. The GCN2-ATF4 pathway is critical for tumour cell survival and proliferation in response to nutrient deprivation. EMBO J 2010;29(12):2082–96 doi 10.1038/emboj.2010.81. [PubMed: 20473272]
42. Ghosh R, Lipson KL, Sargent KE, Mercurio AM, Hunt JS, Ron D, et al. Transcriptional regulation of VEGF-A by the unfolded protein response pathway. PLoS One 2010;5(3):e9575 doi 10.1371/journal.pone.0009575. [PubMed: 20221394]
43. Binet F, Sapieha P. ER Stress and Angiogenesis. Cell metabolism 2015;22(4):560–75 doi 10.1016/j.cmet.2015.07.010. [PubMed: 26278049]
44. Schmitz ML, Shaban MS, Albert BV, Gokcen A, Kracht M. The Crosstalk of Endoplasmic Reticulum (ER) Stress Pathways with NF-kappaB: Complex Mechanisms Relevant for Cancer, Inflammation and Infection. Biomedicines 2018;6(2) doi 10.3390/biomedicines6020058.
45. Tam AB, Mercado EL, Hoffmann A, Niwa M. ER stress activates NF-kappaB by integrating functions of basal IKK activity, IRE1 and PERK. PLoS One 2012;7(10):e45078 doi 10.1371/journal.pone.0045078. [PubMed: 23110043]
46. Oskolkova OV, Afonyushkin T, Leitner A, von Schlieffen E, Gargalovic PS, Lusis AJ, et al. ATF4-dependent transcription is a key mechanism in VEGF up-regulation by oxidized phospholipids: critical role of oxidized sn-2 residues in activation of unfolded protein response. Blood 2008;112(2):330–9 doi 10.1182/blood-2007-09-112870. [PubMed: 18451308]
47. Pereira ER, Frudd K, Awad W, Hendershot LM. Endoplasmic reticulum (ER) stress and hypoxia response pathways interact to potentiate hypoxia-inducible factor 1 (HIF-1) transcriptional activity on targets like vascular endothelial growth factor (VEGF). J Biol Chem 2014;289(6):3352–64 doi 10.1074/jbc.M113.507194. [PubMed: 24347168]

48. Jablonski KA, Amici SA, Webb LM, Ruiz-Rosado Jde D, Popovich PG, Partida-Sanchez S, et al. Novel Markers to Delineate Murine M1 and M2 Macrophages. PLoS One 2015;10(12):e0145342 doi 10.1371/journal.pone.0145342. [PubMed: 26699615]

49. Picelli S, Bjorklund AK, Faridani OR, Sagasser S, Winberg G, Sandberg R. Smart-seq2 for sensitive full-length transcriptome profiling in single cells. Nature methods 2013;10(11):1096–8 doi 10.1038/nmeth.2639. [PubMed: 24056875]

50. N AG, Quintana JA, Garcia-Silva S, Mazariegos M, Gonzalez de la Aleja A, Nicolas-Avila JA, et al. Phagocytosis imprints heterogeneity in tissue-resident macrophages. J Exp Med 2017;214(5): 1281–96 doi 10.1084/jem.20161375. [PubMed: 28432199]

51. Fadok VA, Warner ML, Bratton DL, Henson PM. CD36 is required for phagocytosis of apoptotic cells by human macrophages that use either a phosphatidylserine receptor or the vitronectin receptor (alpha v beta 3). J Immunol 1998;161(11):6250–7. [PubMed: 9834113]

52. Campana D Minimal residual disease in acute lymphoblastic leukemia. Hematology Am Soc Hematol Educ Program 2010;2010:7–12 doi 10.1182/asheducation-2010.1.7. [PubMed: 21239764]

53. Ignatiadis M, Reinholz M. Minimal residual disease and circulating tumor cells in breast cancer. Breast Cancer Res 2011;13(5):222 doi 10.1186/bcr2906. [PubMed: 22078011]

54. Roghanian A, Teige I, Martensson L, Cox KL, Kovacek M, Ljungars A, et al. Antagonistic human FcgammaRIIB (CD32B) antibodies have anti-tumor activity and overcome resistance to antibody therapy in vivo. Cancer Cell 2015;27(4):473–88 doi 10.1016/j.ccell.2015.03.005. [PubMed: 25873171]

55. Dahal LN, Dou L, Hussain K, Liu R, Earley A, Cox KL, et al. STING Activation Reverses Lymphoma-Mediated Resistance to Antibody Immunotherapy. Cancer research 2017;77(13): 3619–31 doi 10.1158/0008-5472.CAN-16-2784. [PubMed: 28512240]

56. Hubert P, Heitzmann A, Viel S, Nicolas A, Sastre-Garau X, Oppezzo P, et al. Antibody-dependent cell cytotoxicity synapses form in mice during tumor-specific antibody immunotherapy. Cancer research 2011;71(15):5134–43 doi 10.1158/0008-5472.CAN-10-4222. [PubMed: 21697279]

57. Zhou GH, Teicher BA, Frei E 3rd. Postlabeling detection of DNA adducts of antitumor alkylating agents. Cancer Chemother Pharmacol 1996;38(1):71–80. [PubMed: 8603455]

58. Warwick GP. The Mechanism of Action of Alkylating Agents. Cancer research 1963;23:1315–33. [PubMed: 14070386]

59. Overdijk MB, Verploegen S, Ortiz Buijsse A, Vink T, Leusen JH, Bleeker WK, et al. Crosstalk between human IgG isotypes and murine effector cells. J Immunol 2012;189(7):3430–8 doi 10.4049/jimmunol.1200356. [PubMed: 22956577]

Significance

Monoclonal antibodies are effective against only a small subset of cancers. Herein we recapitulate compartment-specific antibody resistance and define an ER stress-dependent mechanism induced by high-dose alkylating agents that promotes phagocytosis of opsonized tumor cells. This approach induces synergistic effects with monoclonal antibodies and merits testing across additional tumor types.

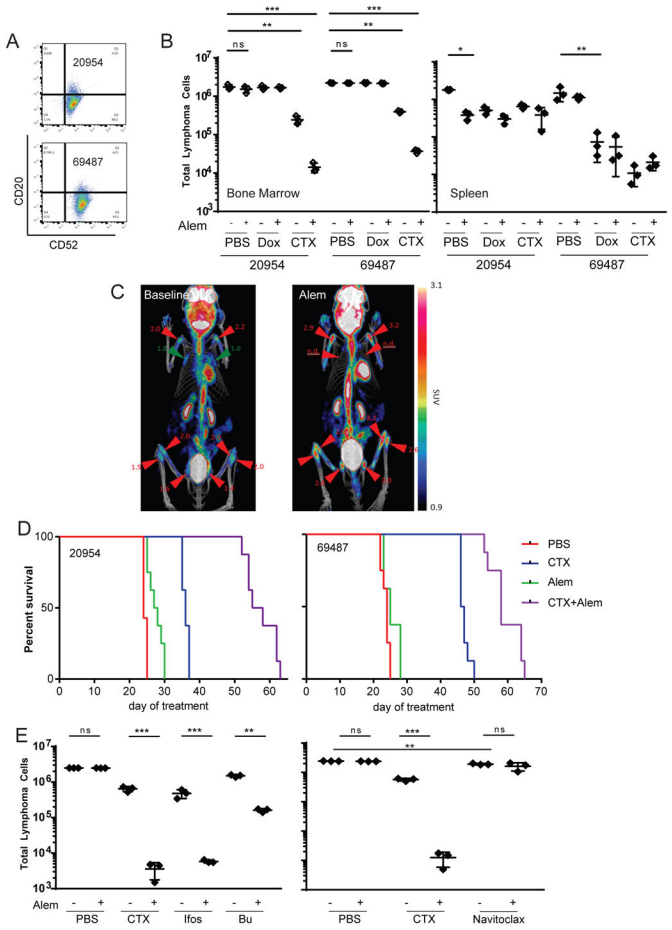

Figure 1: Alkylating Agents Overcome Bone Marrow Antibody Resistance

(A) Flow cytometric analysis of surface CD20 and CD52 expression on DFBL-20954 and DFBL-69487.

(B) On day 8 of treatment, spleen was harvested and a single femur was flushed from mice treated with PBS, Cyclophosphamide (CTX), Doxorubicin (Dox) Alem (Alem) or combinations, as indicated. Total cells were counted and analyzed for the indicated markers. Total tumor cells present are represented as the product of total cells * viable (7-AAD$^-$) hCD19/hCD45 double positive cells. BM tumor burden is represented as the average number of tumor cells per femur. All comparisons by two-sided Welch *t*-test, *p<0.05, **p<0.01, ***p<0.001.

(C) ^{18}FDG-PET imaging of mice engrafted with DFBL-20954 at day 21 post injection (left) and 48 hours after Alem treatment (right) shows progression of disease in bone marrow (e.g. femurs and tibia) but resolution of disease in lymph node regions (e.g. in the axillae).

(D) Kaplan-Meier curves of overall survival of NSG mice engrafted with DFBL-20954 and DFBL-69487 treated with PBS, CTX, Alem or CTX+Alem. p <0.0001 CTX vs Veh, p<0.001 CTX+Alem vs CTX for 20954, p<0.001 CTX+Alem vs CTX for 69487, p<0.001 for CTX+Alem vs. CTX for both. All comparisons by log-rank test.

(E) Bone marrow tumor burden of NSG mice engrafted with DFBL-20954 and treated with PBS, Alem, CTX, ifosfamide (ifos), busulfan (bu) or Navitoclax. Total tumor burden was assessed from one femur as in (B). All comparisons by two-sided Welch *t*-test.

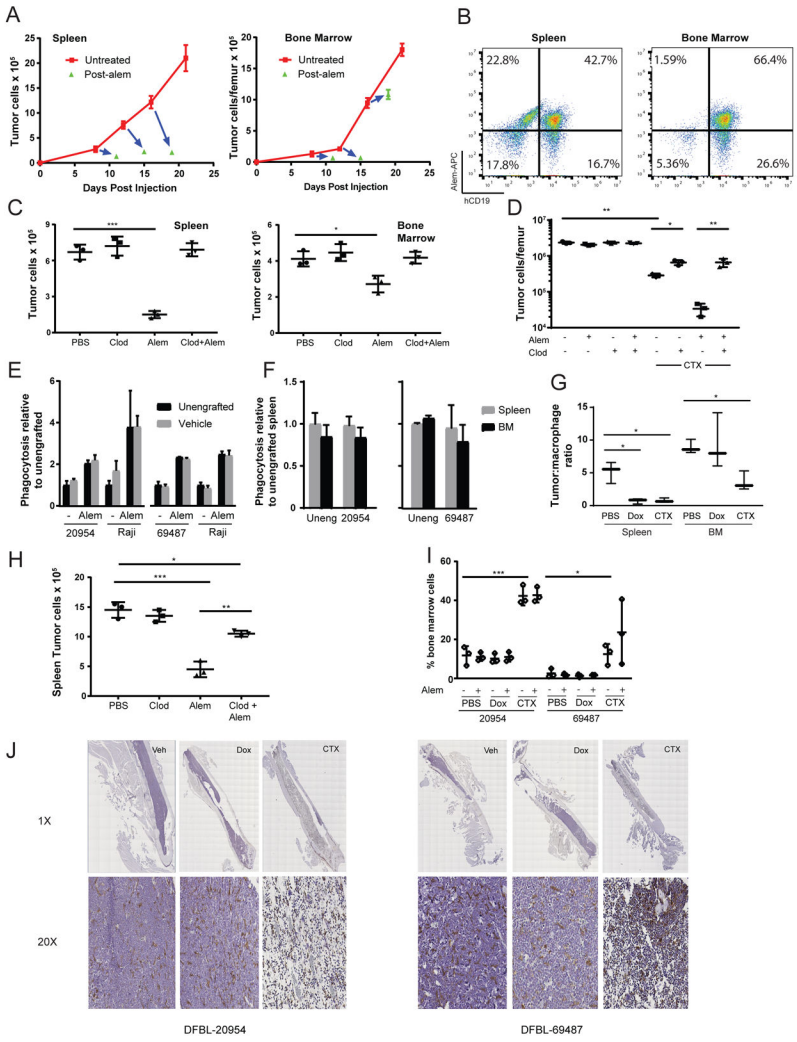

Figure 2: Bone Marrow Resistance to Alemtuzumab Involves Microenvironmental Remodeling

(A) 1×10^6 DFBL-20954 cells were injected into NSG mice and Alem treatment (daily x 2) was initiated on the indicated days 8, 12 and 16 (base of blue arrows). The tips of the blue arrows correspond to tumor burden of mice treated with Alem at 48 hours after the second treatment dose. N=3 mice for each condition at each time point.

(B) Assessment of DFBL-20954 lymphoma cells after *in vivo* treatment with APC-conjugated Alem. Representative flow cytometry plots shown.

(C) On day 10 after transplant of 1×10^6 DFBL-20954 cells, mice were treated with clodronate liposomes (clod, 200ul) or PBS. Alem (Alem) was given as a single dose of 10mg/kg i.v. on day 12. Tumor burden was assessed 48 hours after treatment. Two-sided Welch *t*-test, *p<0.05, **p<0.01, ***p<0.001.

(D) On day 19 after transplant of 10^6 DFBL-20954 cells, mice received clodronate or PBS (−). On day 21, mice received CTX, Alem (10mg/kg i.v. single dose), the combination or vehicle (PBS) and assessed for tumor burden on day 23. Mouse cells were depleted and human cell numbers and viability were assessed with trypan blue staining. Tumor burden is reported as the number of viable tumor cells. Two-sided Welch *t*-test.

(E) Primary, viable BM (7-AAD^{-}hCD19^{-}CD11b^{+}F4/80^{+}) monocytes/macrophages were sorted from unengrafted or lymphoma-engrafted NSG mice. Bone marrow tumor cells from corresponding engrafted mice or Raji cells were incubated in the presence or absence of Alem. All comparisons between unengrafted and vehicle under the same conditions (n=3 per condition) were non-significant.

(F) Primary viable splenic (7AAD^{-}hCD19^{-}CD11b^{-}F4/80^{+}) and BM (hCD19^{-}CD11b^{+}F4/80^{+}) monocytes/macrophages were sorted from unengrafted or lymphoma-engrafted NSG mice and cultured with BM lymphoma cells from the corresponding xenograft that were treated *ex vivo* with Alem. All comparisons between splenic and BM macrophages under the same conditions (n=3 per condition) were non-significant.

(G) Ratio of lymphoma (hCD19^{+}hCD45^{+}) to macrophage (hCD19^{-}CD11b^{-}F4/80^{+}) cells 48 hours after chemotherapy initiation of DFBL-20954-engrafted mice. Two-sided Welch *t*-test, *p<0.05, **p<0.01, ***p<0.001. Dox vs CTX BM Not significant

(H) Mice were engrafted with DFBL-20954 and given clodronate (25ul) or vehicle on day 19 followed by Alem or vehicle on day 21 and 22 and then sacrificed 48 hours after dosing. Spleen tumor burden shown. Two-sided Welch *t*-test, *p<0.05, **p<0.01, ***p<0.001.

(I) Macrophage BM (hCD19^{-}CD11b^{+}F4/80^{+}) cellularity based on flow cytometry 8 days after initiation of the indicated agents. Two-sided Welch *t*-test, *p<0.05, **p<0.01, ***p<0.001. Comparison of PBS vs CTX shown for both xenografts. CTX vs Dox across all conditions significant (p<0.001 for DFBL-20954 and p<0.05 for DFBL-69487).

(J) Representative anti-F4/80 staining (brown) of fixed femurs from mice engrafted with DFBL-20954 or DFBL-69487 and harvested 40 hours after treatment with the indicated agents. Images are 1x and 20x magnified as indicated.

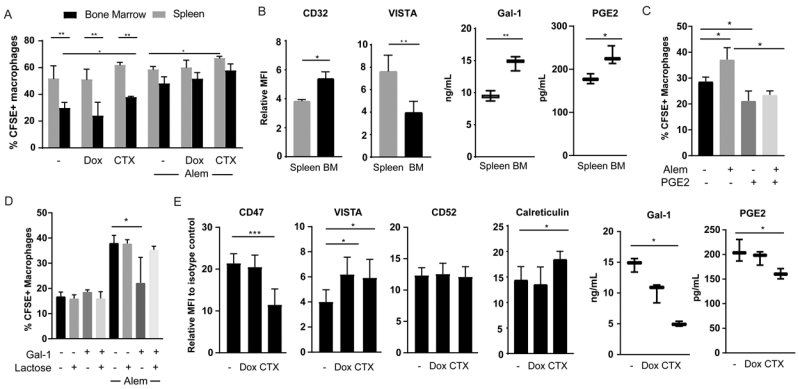

Figure 3: Cyclophosphamide Promotes Lymphoma Phagocytosis by Macrophages

(A) Tumor cells from the spleen and BM of mice (n=3 per condition) engrafted with DFBL-20954 were isolated by mouse cell depletion 16 hours after treatment with PBS, doxorubicin (Dox), or cyclophosphamide (CTX). Dead cells were removed and the remaining live tumor cells were incubated *ex vivo* with bone marrow-derived macrophages in the presence and absence of Alem (Alem). Two-sided Welch's *t*-test, *p<0.05, **p<0.01, ***p<0.001

(B) Surface expression by mean fluorescence intensity (MFI) compared to isotype control or total protein level by ELISA for the indicated proteins in the bone marrow and spleen of DFBL-20954-engrafted mice (n=3-6 per condition). Paired two-sided *t*-test.

(C) DFBL-20954 cells (N=3 mice) were isolated from BM of untreated mice, labeled with CFSE and co-cultured with bone-marrow derived macrophages in the presence or absence of Alem and Prostaglandin E2 (PGE2, 2ng/ml). Phagocytosis was quantified as percent of $CD11b^+$ cells that were $CFSE^+$. The experiment was performed three times and a representative example is shown.

(D) As in (C) but with recombinant human galectin-1 (Gal-1, 500 ng/ml) and lactose (20 mM).

(E) DFBL-20954 engrafted mice (n=3-6 per condition) were treated with the indicated agents and assayed for surface expression of the indicated markers on viable tumor cells. CD47 and VISTA were quantified at 16 hours post-treatment; CD52 and Calreticulin at 48 hours post-treatment. PGE2 and Gal-1 levels were quantified by ELISA 48 hours post-treatment.

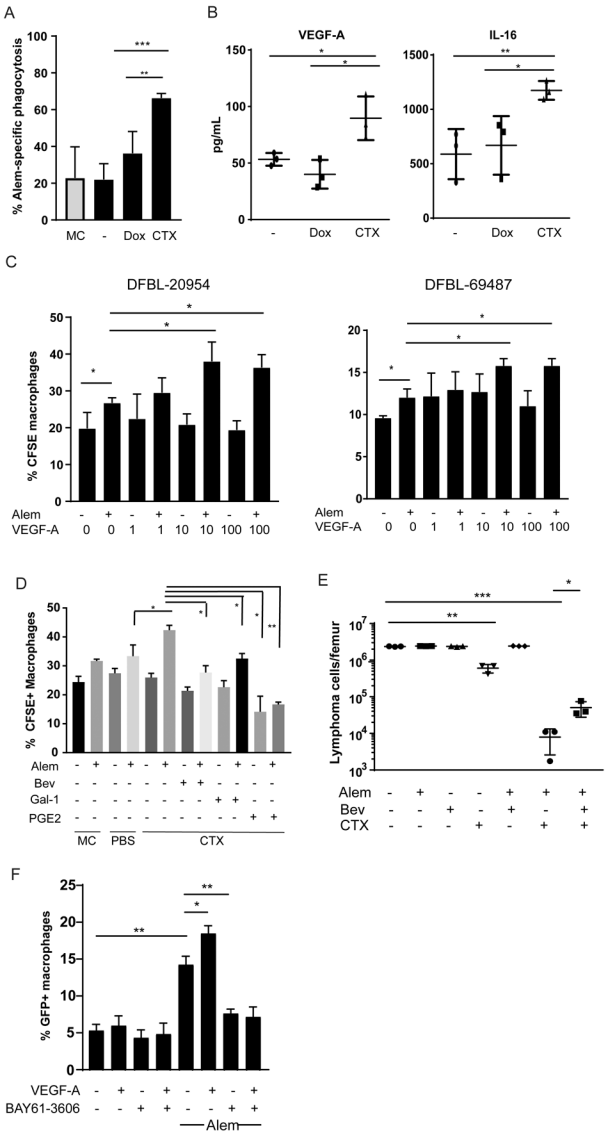

Figure 4: Cyclophosphamide Induces DHL Secretion of VEGF-A and IL-16 to promote tumor clearance

(A) DFBL-20954 cells were isolated from BM of untreated mice, labeled with CFSE and co-cultured with bone-marrow derived macrophages and conditioned media from mice (n=3 per condition) treated as indicated. MC = media control. Alem specific killing is defined as the % increase in $CFSE^+$ macrophages in the presence of Alem compared to no antibody. Unpaired two-sided-*t*-test, **p<0.01, ***p<0.001

(B) Levels of human VEGF-A and IL-16 from bone marrow of DFBL-20954-engrafted mice collected 16 hours after *in vivo* treatment with vehicle (−), doxorubicin (Dox) or cyclophosphamide (CTX). Representative experiment shown. Levels of murine VEGF-A by the same cytokine arrays were <1 pg/ml. Unpaired two-sided-*t*-test, *p<0.05, **p<0.01.

(C) BMDMs were incubated with CFSE-labeled BM lymphoma cells (N=3 mice) from untreated mice supplemented with Alem, recombinant human VEGF-A or vehicle (−). Experiments were performed ≥2 times and representative examples are shown. Phagocytosis

was assessed as the percent of $CD11b^+$ cells that were $CFSE^+$. Two-sided Welch's *t*-test, *p<0.05.

(D) BMDMs were incubated with CFSE-labeled BM lymphoma cells from untreated mice and conditioned media (n=3 mice per condition) supplemented with vehicle (−), Alem, recombinant Gal-1 (1 ¼g/ml), PGE2 (5 ng/ml), and/or bevacizumab (bev, 30 ¼g/ml). Unpaired two-sided-*t*-test.

(E) Bone marrow tumor burden of DFBL-20954-engrafted mice on day 8 after treatment with the indicated agents. Two-sided Welch *t*-test.

(F) BMDMs were incubated with GFP^+ Raji cells and recombinant human VEGF-A (10ng/ml) in the presence and absence of Alem. The experiment was performed three times and a representative example is shown. The SYK inhibitor BAY61-3606 (20 nM) was added as indicated. Phagocytosis was assessed as the percent of $CD11b^+$ cells that were GFP^+. Unpaired two-sided-*t*-test.

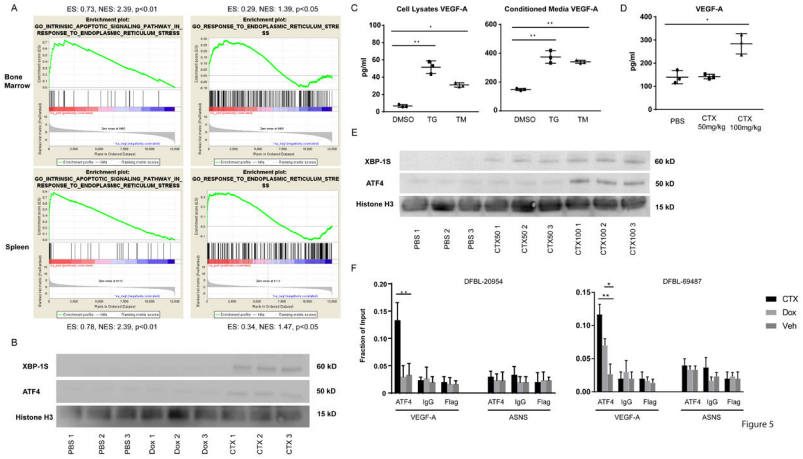

Figure 5: Cyclophosphamide Induces ER Stress in DHL cells that Drives Cytokine Secretion

(A) Gene-set enrichment analysis (GSEA) of ER-stress signatures from RNA sequencing of DFBL-20954 cells collected from spleens or BM. The comparison reflects genes overexpressed after cyclophosphamide (CTX) treatment as compared to PBS treatment. P-values have a false discovery rate (FDR) adjustment. Abbreviations: ES, enrichment score; NES, normalized enrichment score.

(B) Immunoblotting for the indicated targets using lysates from purified, viable BM DFBL-20954 cells collected 16 hours after *in vivo* treatment with PBS (vehicle), doxorubicin (Dox) or CTX. Each lane represents an individual mouse.

(C) Levels of human VEGF-A in cells (left) or media (right) of DFBL-20954 cells isolated from BM and treated *ex vivo* for 24 hours with DMSO, thapsigargin (TG) or tunicamycin (TM). Two-sided Welch *t*-test * $p<0.05$, ** $p<0.01$.

(D) Levels of human VEGF-A from whole BM collected 16 hours after *in vivo* treatment of DFBL-20954-engrafted mice as indicated. Unpaired two-sided-*t*-test.

(E) Immunoblotting, as in (B)

(F) ChIP-qPCR of ATF4 localization to exon 1 of human *VEGF-A* or exon 7 of human *ASNS* in purified, viable BM DFBL-20954 and DFBL-69487 cells collected 16 and 48 hours, respectively, after treatment with Veh, Dox or CTX (n=3 replicates per condition with multiple mice pooled for each replicate). Unpaired two-sided-*t*-test.

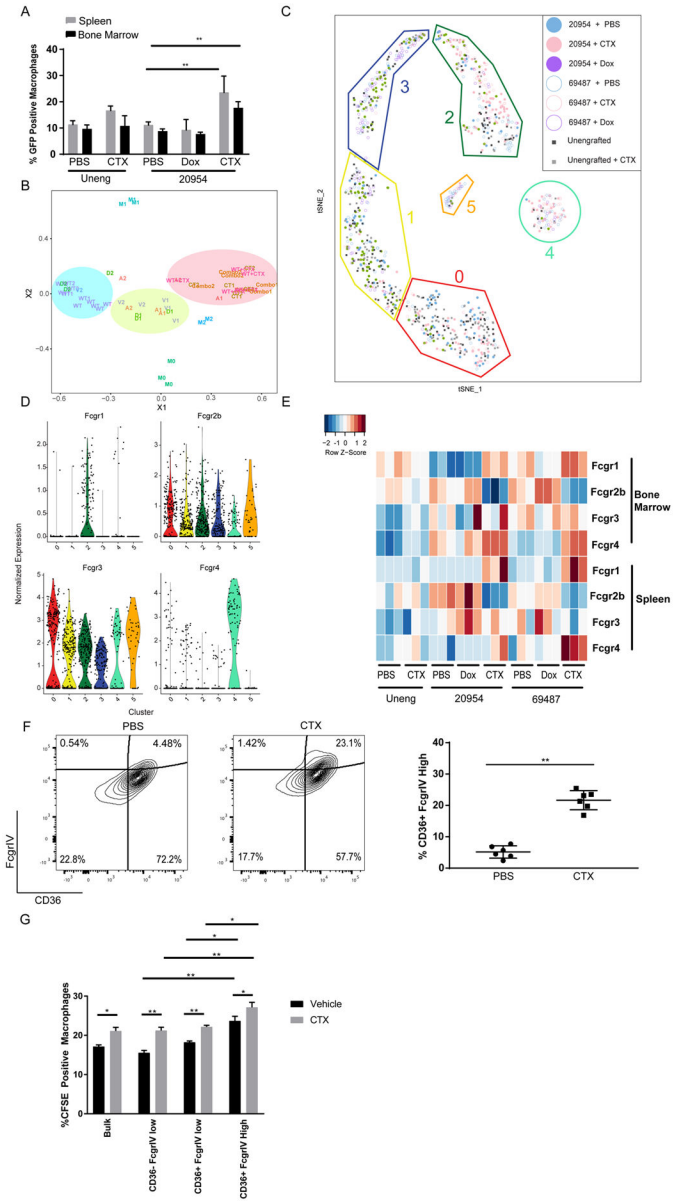

Figure 6: Cyclophosphamide Induces Super-Phagocytic Macrophages in Lymphoma-Engrafted Bone Marrow.

(A) Primary viable splenic (7AAD^{-}hCD19^{-}CD11b^{-}F4/80^{+}) and BM (7AAD $^{-}$hCD19^{-}CD11b^{+}F4/80^{+}) monocytes/macrophages were sorted from unengrafted or DFBL-20954-bearing NSG mice (n=3 per condition) treated with PBS (Veh), doxorubicin (dox) or cyclophosphamide (CTX) and cultured in the presence of GFP^{+} Raji cells that were pre-treated with Alem. Two-sided Welch *t*-test ** p<0.01.

(B) Multidimensional scaling (MDS) analysis of RNA-seq from BM macrophages comparing unengrafted (WT) or lymphoma-engrafted (DFBL-69487=1, DFBL-20954=2) mice treated with PBS (V), Dox (D), Ctx (C), Alem (Alem) or CTX+Alem (combo). Macrophages were harvested 48 hours after treatment.

(C) t-SNE plot of single-cell RNA-seq of BM macrophages from unengrafted (uneng) or engrafted mice treated with PBS, dox or CTX shows six clusters (left). Cluster 4 is enriched with macrophages from CTX-treated, lymphoma-engrafted mice. Clusters and numbers in each cluster from each treatment group are indicated in the figure legend.
(D) Expression of Fc-gamma receptors from single-cell RNA-seq of sorted BM macrophages clustered as in (C).
(E) Flow-cytometric analysis of Fc-gamma receptor expression on macrophages from unengrafted or DFBL-29054-engrafted mice treated *in vivo* as indicated. Macrophages were collected 48 hours after treatment. Heatmap represents Z-scores of MFIs normalized to isotype controls.
(F) Representative flow cytometry of BM macrophages collected from DFBL-29054-engrafted mice treated with PBS or CTX. Unpaired two-sided-*t*-test
(G) Macrophages from (F) were sorted as indicated or unsorted (Bulk), labelled with CFSE and exposed to BM DFBL-20954 cells from mice treated with PBS or CTX that were pre-treated *ex vivo* with Alem (n=5 mice per condition). Unpaired two-sided-*t*-test, *$p<0.05$, **$p<0.01$